Journal of Catalysis 271 (2010) 1–11

Contents lists available at ScienceDirect

Journal of Catalysis

journal homepage: www.elsevier.com/locate/jcat

Fe-H-BEA and Fe-H-ZSM-5 for NO_2 removal from ambient air – A detailed in situ and operando FTIR study revealing an unexpected positive water-effect

Mike Ahrens [1], Olivier Marie *, Philippe Bazin, Marco Daturi

Laboratoire Catalyse et Spectrochimie, ENSICAEN, Univ. Caen, CNRS, 6 Bd Maréchal Juin, F-14050 Caen, France

ARTICLE INFO

Article history:
Received 4 December 2009
Revised 12 January 2010
Accepted 21 January 2010
Available online 11 March 2010

Keywords:
Iron
Zeolite BEA ZSM-5
NO_2 removal
Ambient air
In situ FTIR
Operando FTIR
Water-effect

ABSTRACT

The NO_2 removal performance of Fe-modified H-BEA and H-ZSM-5 has been investigated in detail by means of in situ and operando FTIR spectroscopy. The surface characterization using NO_2 and NO as probe molecules revealed important contributions of redox processes involving Fe^{3+}-OH and/or α-oxygen species as well as Fe^{2+}-NO species. In these anhydrous conditions, the NO_2 storage performance is mainly due to the disproportion of NO_2 leading to NO^+ and nitrate species. However, under flow and in the presence of humidity, and thus in more realistic conditions, nitrates and NO^+ formation are suppressed. The main mechanism responsible for the wet NO_2 removal consists in the formation of both adsorbed nitric acid and gaseous NO. According to the proposed mechanism, a strong positive water-effect is established: the total suppression of NO_2 in the presence of humidity together with the formation of NO, which is less toxic than NO_2, makes the investigated zeolites promising candidates for efficient materials used in indoor air treatment.

1. Introduction

Considering the very general frame of gaseous pollutant removal from ambient air, many efforts have been made during the last decades in order to develop not only filtration/adsorption devices [1–4] but also systems able to convert harmful molecule traces (within the ppb–ppm concentration range) into less harmful ones. Among the active systems, both chemical solutions [5–7], catalytic [8], photocatalytic [9–16] and plasma-assisted technologies [17,18] have emerged, and the combination of adsorbents and active systems often appears to be necessary in order to improve the efficiency for a broad range of pollutant targets in the ambient air conditions [14,19,20].

Fore sure, the efficiency of the cleansing system will depend on several constraints such as the nature of pollutant targets and the environment of the ambient air, i.e. outdoor, indoor, confined atmosphere, etc. This work is part of a more global project aiming at removing several targets (hydrocarbons, aldehydes, NO_x, ...) from indoor air. We decided here to focus on NO_2 which belongs to the most widely measured ambient air quality standards [21] and which is continuously produced in combustion engines. Naturally, the most widely reported active systems for NO_2 elimination from ambient air are based on a photocatalytic process involving TiO_2 materials [9,10,12,15]; however, operating conditions require sunlight or artificial UV–Vis irradiation which is not compatible with an onboard application for example. For the same reason, we also disregarded the plasma processes which are energy demanding and would imply a non-reasonable overcost and over-consuming drawback for vehicle application. We thus focused our attention on zeolites as alternatives to charcoal/activated carbon, since they also possess high adsorption capacities but moreover present the possibility (when transition metal loaded) to catalytically reduce NO_2. Indeed, the choice of Fe-zeolites was suggested by their recent commercial introduction in the NH_3 SCR process for DeNOxing of Diesel vehicles exhausts (thus in presence of water) [22–24], where they lead to high reactivity with NO_2 which boosts the low-temperature deNO_x performances [25]. Two different zeolitic framework types (H-BEA and H-ZSM-5) with different physico-chemical properties were tested after they had been loaded with iron upon ionic exchange. Among the possible transition metal candidates, iron was chosen as a promising provider of active redox centers in ambient air conditions [9,10] furthermore, its low cost was also considered as an interesting parameter.

The first part of this study deals with the investigation into redox active centers in the iron-loaded shaped zeolites (with alumina binder). For this purpose, the samples were first thermally pretreated either under vacuum or oxygen with the subsequent study of the available site interactions with probe molecules. Even if nitrogen dioxide is rarely used for such an application due to its strong reactivity with redox centers thus affecting the nature of

* Corresponding author. Fax: +33 2 31 45 28 22.
E-mail address: olivier.marie@ensicaen.fr (O. Marie).
[1] Current address: Humboldt-Universität zu Berlin, Institut für Chemie, Brook-Taylor Str. 2, 12489 Berlin, Germany.

0021-9517/$ - see front matter © 2010 Elsevier Inc. All rights reserved.
doi:10.1016/j.jcat.2010.01.020

the probed site even at room temperature, we undertook NO_2 adsorption experiments, since this molecule is our reactant. Naturally, the more widely applied probe molecule for redox centers characterization, i.e. NO [26–28], was also adsorbed on our samples for complementary information.

In a second step of this work, the zeolite behaviour in more realistic conditions was investigated. No thermal pre-treatment was thus applied, and the samples were submitted 'as is' to an NO_2 polluted flow at room temperature. Our aim was to determine the NO_2 removal efficiency and selectivity in 'as close as possible' working conditions, and thus the effect of water content was studied as an important parameter [19,20,29]. Our operando set-up, which allows us to observe the zeolite porous system under working conditions, was of a great help to establish the NO_2 removal mechanism in ambient air conditions.

2. Experimental details

The Fe-H-BEA and Fe-H-ZSM-5 were supplied by IRMA and prepared from commercial zeolites by ionic Fe-exchange. In order to study a shaped, finalized adsorbent, 20 wt.% of Al_2O_3 binder has been added to the studied zeolites. The main physico-chemical properties of the shaped samples are given in Table 1.

In situ FTIR spectra have been recorded with a Nicolet Avatar spectrometer in transmission mode using self-supported discs consisting of 10 mg cm^{-2} of the catalyst material. A room temperature IR-cell equipped with a heating device to offer the possibility to activate the catalyst at temperatures up to 800 K has been used. The cell has been connected to a High Vacuum line with a reachable pressure of 10^{-5} Pa, equipped with two ports for the introduction of probe molecules and a calibrated small volume between two valves, providing the possibility to introduce known volumes and thus known amounts of the probe molecules. The detectors used for the FTIR data collection have been either of the DTGS or of the MCT type.

A two-step activation has been used with a first step at 393 K for 1 h to desorb most of the naturally adsorbed water and a second step at 673 K for 1 h to complete the sample thermal treatment. The heating rate was set to 2 K/min. All steps were performed under secondary vacuum. In order to check the importance of the oxidation state of Fe, O_2 (13.3 kPa) was, when desired, introduced at the beginning of the second step. All spectra were recorded at room temperature.

Concerning operando FTIR, an operando cell that allows a constant temperature at 298 K (via a thermostat) and self-supported catalyst-discs (see in situ FTIR) have been used. The cell was connected to the operando gas-system including a Nicolet Magna FTIR spectrometer allowing to record both surface and gas phase spectra (via an additional on-line gas cell). In order to increase sensitivity, detectors were of the MCT type. The exhaust gases were also investigated using quadrupole mass spectrometry (Pfeiffer Omnistar GSD 301) and chemiluminescence (model 42i-HL form Thermo Scientific). In order to establish conditions as close as possible to the working ones, no activation procedure was performed except a short purging period at room temperature before sending the gas mixture.

Table 1
Main physico-chemical properties of studied samples.

Sample	Fe-H-BEA	Fe-H-ZSM-5
Fe-content (wt.%)	0.76	1.6
Si/Al ratio	40	18
Surface area (m^2/g)	528	263
Binder (wt.%)	20 of γ-Al_2O_3	20 of γ-Al_2O_3

For all operando experiments, a total flow of 25 cm^3/min was established. This flow always consisted of Ar and 20% O_2 (to simulate atmospheric conditions) to which NO_2 (diluted in Ar) and the desired percentage of H_2O (0–1.7%) were added. While NO_2 (350 ppm) has been introduced normally in gaseous diluted form, H_2O has been introduced via a saturator using the corresponding Antoine's coefficients to calculate the correct flow and temperature values. NO_2 adsorption capacities have been calculated using the recorded chemiluminescence data, taking into account the flow conditions and the results of the corresponding blank experiment.

3. Results and discussion

3.1. Sample characterization by in situ IR

3.1.1. Activated samples

In Fig. 1, the IR spectra in the OH stretching region of Fe-H-BEA are shown for the two different activation profiles. Regarding the activation under vacuum, four bands with maxima at 3781, 3745, 3663 and 3610 cm^{-1} are present. After activation under oxygen, an additional band at 3683 cm^{-1} is detected. It should be mentioned that this band decreases with increasing evacuation time and is – as for the activation under vacuum – absent for an activation treatment under hydrogen.

According to literature, the band at 3745 cm^{-1} represents external silanols [30–33], while the band at 3610 cm^{-1} arises from acidic Al–O(H)–Si bridged hydroxyl groups [30–32]. Furthermore, OH groups attached to Al-species partially connected to the framework [30,32] (extra-framework Al-species, sometimes said to be non-acidic [31]) give rise to the band at 3663 cm^{-1}. It was described by Vimont et al. [32] that the band at 3781 cm^{-1} may correspond to an OH group with basic properties attached to tricoordinated Al partially connected to the zeolitic framework. Thus, this band can give an indication that the zeolitic framework is destroyed up to a certain extent. Nevertheless, it can not be ruled out completely that this band belongs to an OH group present in pure alumina [34], as Al_2O_3 is present in the samples acting as a binder. Indeed, the spectrum relative to Fe-H-ZSM-5 diluted with the same alumina binder (Fig. 1 spectrum c) presents the same set of bands thus indicating that, except the 3610 cm^{-1} one, the detected peaks should be mainly associated with ν(OH) from Al_2O_3 hydroxyls.

The band at 3683 cm^{-1}, only present after activation under oxygen, corresponds to a Fe^{3+}-OH group. Recently, a detailed FTIR investigation has been performed by Kefirov et al. [35] using CO

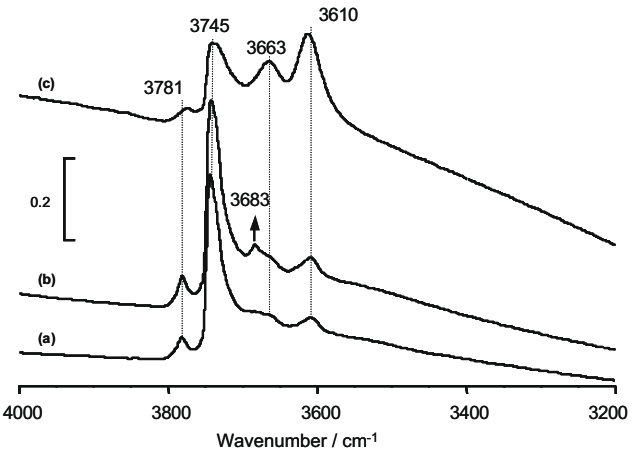

Fig. 1. FTIR spectra of Fe-H-BEA activated at 673 K under vacuum (a) and under O_2 (b) together with spectrum of Fe-H-ZSM-5 activated at 673 K under vacuum (c).

and NO as probe molecules to discuss the relationship of this Fe^{3+}-OH group with so-called α-oxygen.

3.1.2. NO_2 adsorption on Fe-H-BEA

In order to study the reactions taking place upon NO_2 adsorption on Fe-H-BEA, a series of small doses of NO_2 have been added to the sample at room temperature. In Fig. 2, the evolution of the bands in the OH stretching region is shown for the samples activated under vacuum and oxygen, respectively. It can be seen that in both cases, an increase in the band due to Fe^{3+}-OH groups can be observed for the addition of the first small volumes being more distinctive in the case of the sample activated under vacuum (only a small increase in this band can be observed for the oxygen-treated sample). Continuing the adsorption process, the Fe^{3+}-OH sites are next consumed, which can be clearly seen for the oxidized sample from the decrease of the corresponding 3683 cm^{-1} band upon the addition of the following small volumes. For the 'under vacuum' pretreated sample, the consumption of the Fe^{3+}-OH sites takes place in the same way, but the IR spectra do not lead to noticeable negative band at 3683 cm^{-1}, since the 'reference' subtracted spectrum corresponds to the 'after vacuum' recorded one for which no Fe^{3+}-OH group is detected (see Fig. 1). In this case, the 3683 cm^{-1} band first appears and increases before coming back to zero upon the consumption of the initially created Fe^{3+}-OH hydroxyls. Taking into account all other present OH groups, a uniform consumption of these sites can be found for both samples. In the same time, a broad band covering the whole OH region is established, traducing the presence of H_2O interacting with hydroxyls via H-bonding. This finding indicates the formation of H_2O during the adsorption process. A possible explanation for the formation of water during the adsorption process has been given by Hadjiivanov et al. [36] when co-adsorbing O_2 to NO on H-ZSM-5 samples.

Regarding the 2400–1350 cm^{-1} range (Fig. 3), the same features in terms of band positions can be observed for both samples. The addition of small volumes of NO_2 results in an uniform increase in two bands corresponding to adsorbed NO^+ species [27,36–42] (2175 and 2132 cm^{-1}, the former being sometimes associated with NO^+ adsorbed on non-protic sites [27] or with N_2O_4 [37] with a complement 1750 cm^{-1} component in that case) and several bands in the nitro- and nitrate-region (1651, 1635, 1624, 1596 and 1582 cm^{-1}). Focussing on the nitro and nitrate bands, a clear assignment to concrete species tends to be complicated due to quite different data in the literature. For example, the band located at 1624 cm^{-1} can arise either from a bridging Al-nitrate species [43,44] or from a species attached to extra-framework Fe–Al–O [45]. Furthermore, the $\delta(H_2O)$ mode of adsorbed water also lies in this region [36,46]. Nevertheless, consistent information can be found for the bands located at 1651 and 1635 cm^{-1} regarding the nature of the adsorption site, the first representing an Al-based nitro species [45] or alumina-bridged nitrates [44], the latter a nitrate species at least involving Fe in different environments [39,45]. Finally, the lower wavenumber components in this nitro/nitrates region at 1596, 1582 cm^{-1} can be confidently assigned to alumina bidentate and monodentate nitrates, respectively [44]. To summarize, only the 1635 cm^{-1} band can be assigned to an iron-containing nitrate species. An additional band with its maximum at 1874 cm^{-1} indicates the formation of Fe^{2+}-NO species [35,39,45,47]. For both activation methods, this band increases upon the addition of the first small volumes and then decreases and finally vanishes with further equilibrium NO_2 pressure. However, the band maximum intensity for the vacuum-activated sample (see Fig. 3 inset) is around four times higher, thus indicating a much higher amount of Fe^{2+} cations. The band situated at 1746 cm^{-1}, mainly present at higher doses, corresponds to adsorbed N_2O_4 [38].

As already described, the positions of the observed bands are not affected by the activation treatment. But regarding the amount of the formed species, it can be stated that even if the amounts of NO^+ and Al-based nitro species are comparable, both the Fe^{2+}-NO (1874 cm^{-1}) and the iron-based NO_3^- species (1635 cm^{-1}) are more abundant after a vacuum treatment. Furthermore, the final decrease of the Fe^{2+}-NO band corresponds for both pre-treatments to an increase in the relative intensity of the iron-based NO_3^- species which suggests that in NO_2 excess, Fe^{2+} nitrosyl are involved in the formation of nitrates.

Regarding the reactions taking place during the adsorption process, three different pathways should be formulated.

(i) In both activation treatments, the well-known disproportion reaction according to:

$$2NO_2 \rightarrow NO^+ + NO_3^- \quad (1)$$

leading to the formation of adsorbed NO^+ species, and surface nitrates has to be considered.

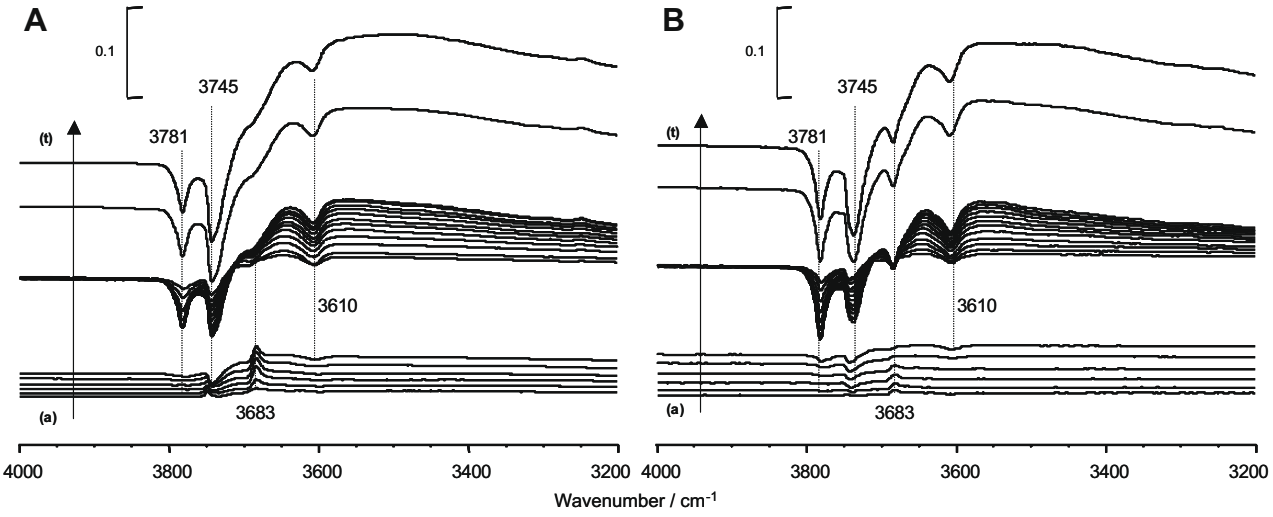

Fig. 2. FTIR spectra in the ν(OH) range taken during the adsorption of NO_2 on Fe-H-BEA activated at 673 K under vacuum (A) and under O_2 (B) with the corresponding amount of introduced probe molecule: from (a) to (f) between 5 and 90 μmol g^{-1}; from (g) to (r) between 100 and 850 μmol g^{-1} and for (s) and (t) with an NO_2 equilibrium pressure of 133 and 266 Pa, respectively.

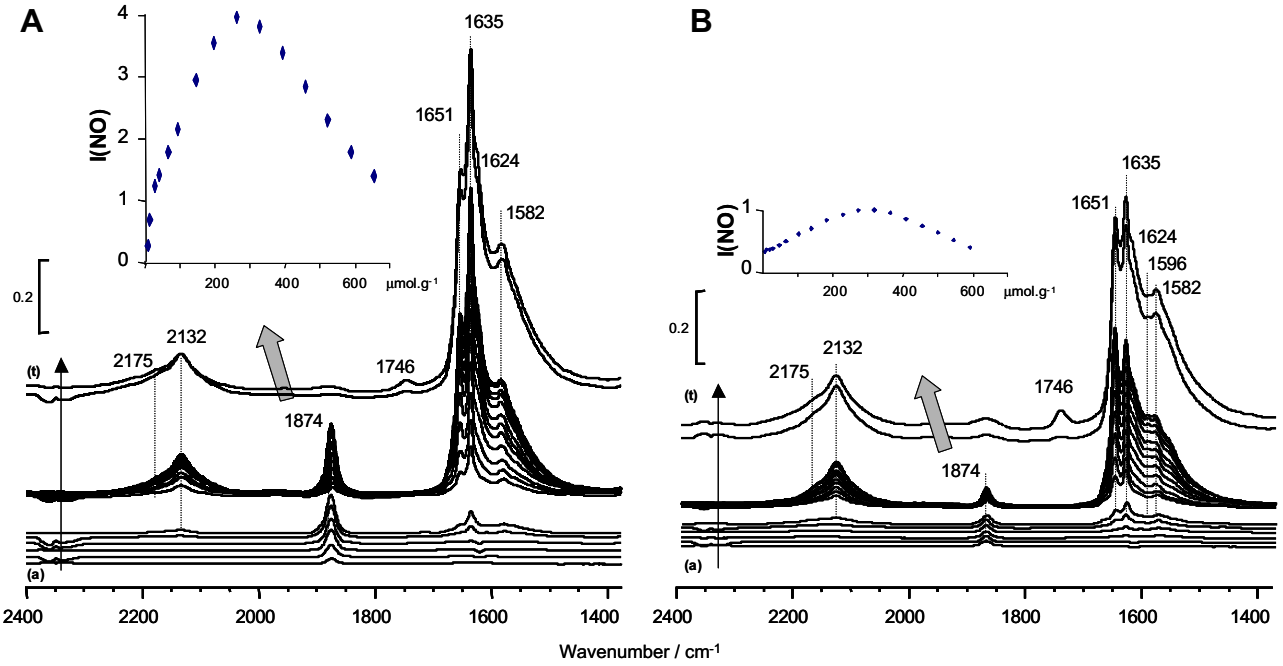

Fig. 3. FTIR spectra in the (2400–1400) range taken during the adsorption of NO_2 on Fe-H-BEA activated at 673 K under vacuum (A) and under O_2 (B) with the corresponding amount of introduced probe molecule: from (a) to (f) between 5 and 90 μmol g^{-1}; from (g) to (r) between 100 and 850 μmol g^{-1} and for (s) and (t) with an NO_2 equilibrium pressure of 133 and 266 Pa, respectively. The two inset plots represent the evolution of the nitrosyl ν(NO) band integrated intensity (expressed in cm^{-1}) versus the amount of introduced NO_2.

(ii) Taking into account the findings from the OH region, the second pathway should be connected to two species, namely the Fe^{3+}-OH and Fe^{2+}-NO groups and thus resulting in a kind of redox process. Nevertheless, this process has to be formulated differently for each activation method used for Fe-H-BEA.

In the case of an activation under vacuum, it can be assumed that a certain amount of Fe^{2+} species is already present in the sample, and the formation of Fe^{2+}-NO species can be formulated according to:

$$2Z\text{-}Fe^{2+} + NO_2 \rightarrow Z\text{-}Fe^{3+}\text{-}O^- + Z\text{-}Fe^{2+}\text{-}NO \quad (2)$$

resulting in the appearance of an Fe^{3+}-OH species from Fe^{3+}-O^- when water is present in the close vicinity or of a ferric nitrate when a supplementary NO_2 molecule adsorbs on Fe^{3+}-O^-. This reaction takes place until all Fe^{2+} is oxidized or occupied by NO. The fact that the Fe^{2+}-NO band decreases and finally disappears upon further addition of NO_2 could be explained by a transformation into a Fe^{3+}-nitrate species. This would explain why the nitrate at 1635 cm^{-1} still increases uniformly while all other bands in that region start to saturate. Similar observations concerning the transformation of Fe^{2+}-NO species into ferric nitrate species have been made by Kefirov et al. [35] and Mul et al. [39] using Fe-BEA and Fe-ZSM-5, respectively.

Considering an activation under oxygen, the amount of Fe^{2+} species present after activation should be lower and possibly negligible. We thus looked for a possible path to generate Fe^{2+}-NO species from Fe^{3+} reduction. The biggest difference, when compared with the activation under vacuum, is surely the behaviour of the Fe^{3+}-OH group: it is already present after activation and further consumed during the adsorption process. It can be assumed from literature that this group is quite reactive and also easy to reduce; a possible way to form Fe^{2+} can be formulated according to:

$$Z\text{-}Fe^{3+}\text{-}OH + NO_2 \rightarrow Z\text{-}Fe^{2+} + H^+NO_3 \quad (3)$$

able to deliver an additional nitrate source and to explain the consumption of Fe^{3+}-OH and the formation of Fe^{2+}-NO. However, NO_2 is a rather strong oxidizing agent, and we have no proof that Z-Fe^{3+}-OH groups are stronger ones, which is a prerequisite to satisfy Eq. (3). An alternative explanation lies in the reaction of NO [which could form from residual Fe^{2+} species according to Eq. (2)] with Fe^{3+}-OH as further discussed [see Eq. (5)].

(iii) The third pathway consists in the reaction of NO_2 and NO with Brønsted acid OH groups of the zeolites according to the following equation [36]:

$$2Z\text{-}OH + NO_2 + NO \rightarrow 2Z\text{-}O^-NO^+ + H_2O \quad (4)$$

as evidenced by the consumption of bridged OH groups upon NO_2 adsorption.

When comparing the two activation procedures, it can be stated that Fe^{3+}-OH plays an important role in the adsorption process of NO_2 on Fe-H-BEA representing a possible reaction product in the presence of water for Fe^{2+}-rich and a reactant for Fe^{2+}-poor samples.

3.1.3. NO adsorption on Fe-H-BEA

In order to obtain more information on the redox process involving Fe^{3+}-OH and Fe^{2+}-NO during the adsorption of NO_2, NO has been used as a probe molecule. Due to the initial absence of NO_2, the formation of NO^+ and NO_3^- species should be inhibited and thus, the redox process could be investigated alone. The corresponding spectra for both activation methods are shown in Fig. 4, in the [2200–1350 cm^{-1}] range and in the OH stretching region (only for Fe-H-BEA activated under O_2). Regarding Fe-H-BEA activated under vacuum, an increasing band at 1874 cm^{-1} indicates the formation of a Fe^{2+}-NO species [39,45,47] upon the addition of small volumes of NO. As already noticed from the NO_2 adsorption experiments, enough Fe^{2+} species should be present after vacuum treatment to enable the formation of such species. At higher

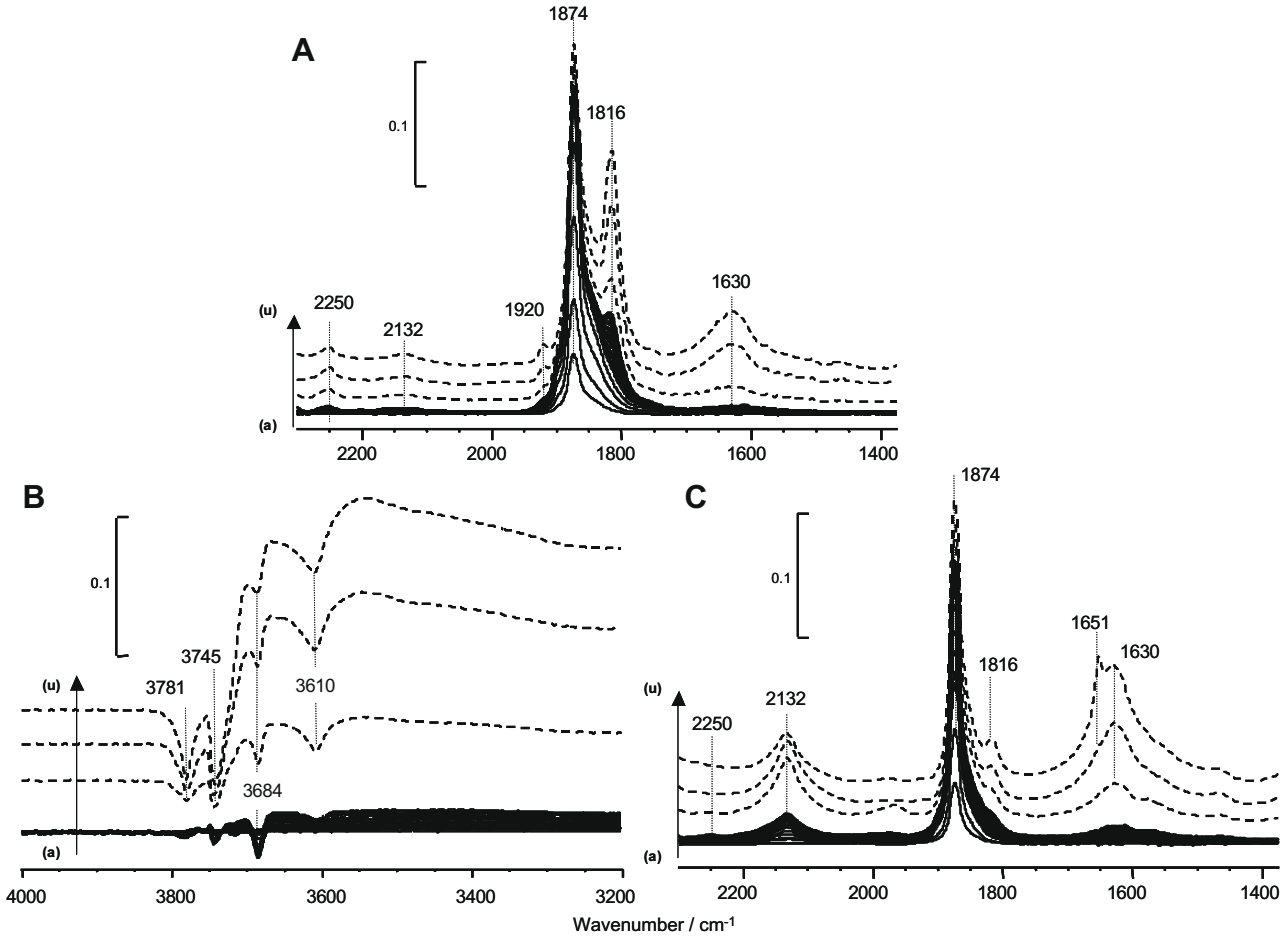

Fig. 4. FTIR spectra taken during the adsorption of NO on Fe-H-BEA activated at 673 K under vacuum (A) and under O_2 (B) and (C) with the corresponding amount of introduced probe molecule: from (a) to (r) between 6 and 700 μmol g^{-1} and for (s), (t) and (u) with an NO equilibrium pressure of 133, 400 and 665 Pa, respectively.

NO-doses, a second band at 1816 cm^{-1} develops which can be assigned to poly-NO species, the shoulder around 1920 cm^{-1} being a confirmation for this assignment [47]. For this vacuum activation method, it can be assumed that unsaturated Fe^{2+} species are present in the sample providing the ability to adsorb more than one NO molecule per Fe^{2+} cation. The presence of these unsaturated Fe^{2+} species able to adsorb two NO molecules in a very close neighbourhood may justify the observation of adsorbed N_2O (2250 cm^{-1}) whose formation is hindered with the O_2 pre-treated zeolite.

Although the band positions found for the sample activated under oxygen tend to be similar in the 2200–1350 cm^{-1} region (when compared with the vacuum treatment), the processes taking place on that sample have to be described differently. Indeed, even if it is not possible to rule out that a certain amount of Fe^{2+} species is still present in the sample after an activation under oxygen, we looked for a possible mechanism generating Fe^{2+} species in order to explain the still rather intense component at 1874 cm^{-1} typical of Fe^{2+}-NO species. According to Kefirov et al. [35], this should be possible via:

$$Z\text{-}Fe^{3+}\text{-}OH + NO \rightarrow Z\text{-}Fe^{2+} + H^+NO_2 \quad (5)$$

$$H^+NO_2 + Z\text{-}OH \rightarrow Z\text{-}O\text{-}NO^+ + H_2O \quad (6)$$

This mechanism involving Fe^{3+}-OH and other acidic OH groups present in the sample is consistent with the findings made here for the sample activated under O_2: it explains the initial high reactivity of the Fe^{3+}-OH (see 3684 cm^{-1} band on Fig. 4B) and later of the acidic-bridged OH groups (3610 cm^{-1}) together with the formation of water (around 1630 cm^{-1} in the nitrate region) and of higher amount of NO^+ species (when compared with vacuum pre-treated sample) upon the adsorption process. It should be mentioned that for the vacuum-activated sample, OH species are only involved in the adsorption process at the highest doses (not shown here). The formation of poly-NO species is less obvious in the case of the oxygen-treated sample due to the smaller amount of unsaturated Fe^{2+} species after such a treatment. Regarding the nitrate region, we only observe the formation of species upon prolonged time under NO equilibrium pressure.

Indeed, the Fig. 5A reports the band evolution upon time of the sample treated with oxygen under an equilibrium pressure of NO (665 Pa) in the range 2200–1350 cm^{-1}. An increase in the bands in the nitrate region together with no substantial changes for NO^+ and Fe^{2+}-NO can be established. This behaviour is only present for the oxygen-treated sample. It should be mentioned that the most dominant feature can be found at 1651 cm^{-1} corresponding most probably to NO_2 adsorbed on Al-sites [45]. Some other bands at lower wavenumber (1624–1557 cm^{-1}) develop, which indicate the formation of alumina nitrate species. Two pathways should be considered for the nitrate formation, the first being the already mentioned transformation of Fe^{2+}-NO species into ferric nitrate species [35]. The second one would involve the generation of NO_2 via a process consuming α-oxygen-containing species according to:

$$Z\text{-}Fe^{3+}\text{-}O^- + NO \rightarrow Z\text{-}Fe^{2+} + NO_2 \quad (7)$$

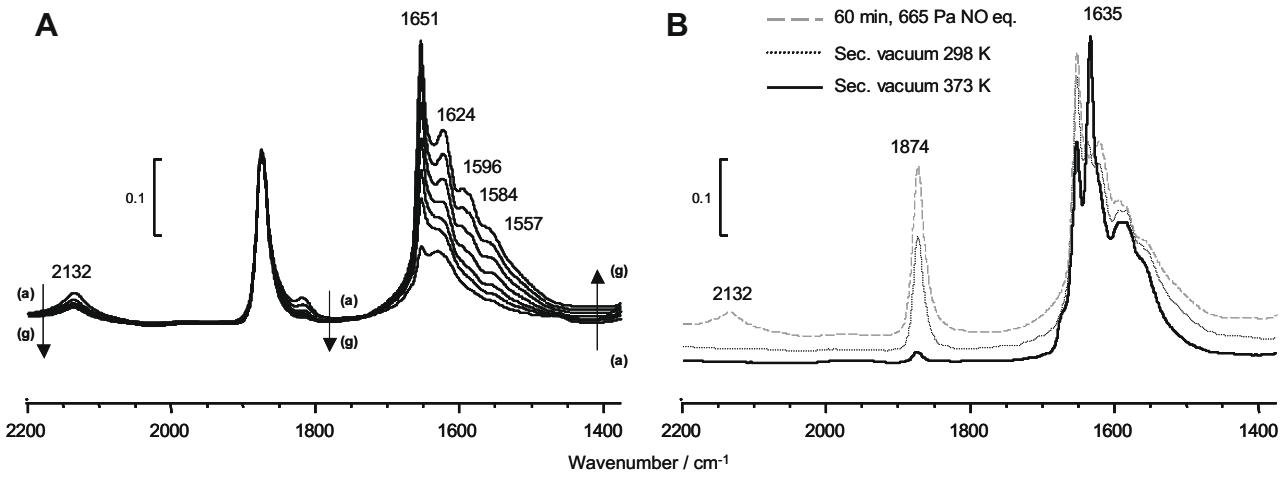

Fig. 5. (A) FTIR band evolution upon time after addition of 665 Pa equilibrium pressure of NO for Fe-H-BEA activated under O_2: from (a) to (g) each spectrum is separated by a 10-min interval under NO equilibrium pressure and (B) Evolution of spectra after further thermal desorption.

As soon as NO_2 is present, the NO^+ and nitrate formation via the NO_2 disproportion proceeds. In fact, the possibility to form NO_2 from the reaction of NO with reactive O-species is necessary to explain the early observation of NO_2 adsorbed on Al-sites and the further formation of alumina nitrate species. The fact that no further increase in the NO^+ band can be found may be due to an interaction of water with those species. Desorbing the adsorbed species (Fig. 5B) leads to the already mentioned transformation of Fe^{2+}-NO into a nitrate species at 1635 cm^{-1}, confirming the assignment of this band to an Fe-containing nitrate species [39]. It should be mentioned that the originally consumed Fe^{3+}-OH species is regenerated around 573 K (not shown), and thus is consistent with literature data.

4. Combining results from in situ NO_2 and NO adsorption

The most obvious difference between vacuum- and oxygen-treated Fe-H-BEA upon NO_2 adsorption is the amount of Fe^{2+}-NO and the changed ratio of the nitro/nitrate features at 1651 and 1635 cm^{-1}. Taking into account the results obtained from NO adsorption on both pre-treated samples, it can be stated that the presence of active O-species (Fe^{3+}-OH and/or α-oxygen) in the case of an activation in the presence of oxygen provides an additional source for the formation of NO_2 which further converts into NO^+ and NO_3^-. Furthermore, the evolution of the nitro/nitrate bands under an equilibrium pressure of NO with time (for an O_2 pre-treated sample) also traduces that different species are involved: the band at 1651 cm^{-1} is the dominant one, while the band at 1635 cm^{-1} is absent in that case. The former being typical of Al-based nitro species, it can be stated that NO_2 is first obtained from the active O-species and then diffuses to lead to nitrate species over the neighbouring alumina binder. On another hand, the 1635 cm^{-1} band is associated with the presence of Fe^{2+}-NO species and becomes the dominant component in the nitro/nitrate region when these iron nitrosyls are consumed (either upon NO_2 adsorption or NO evacuation). To summarize, under NO equilibrium pressure, iron sites are mobilized to yield NO_2 which further reacts preferentially with alumina, while under NO_2 equilibrium pressure iron sites are more readily involved to yield ferric nitrates.

4.1. Main results on Fe-H-ZSM-5

The same kind of experiments were conduced over the Fe-H-ZSM-5 sample, and Fig. 6 reports the spectra obtained from the adsorption of NO_2 at room temperature after an activation under vacuum. In principle, the same conclusions can be drawn for this sample as for the Fe-H-BEA one, i.e. both reaction pathways (disproportion and redox reaction) are taking place.

Nevertheless, a few important differences can be found. The most obvious difference is the finding that the Fe^{2+}-NO band is heterogeneous and indeed made of two species (1890 and 1879 cm^{-1}) and does not decrease completely upon higher doses, even with an NO_2 equilibrium pressure (see Fig. 6B and inset). In this Fe-H-ZSM-5 sample, all the Fe^{2+} species are thus not readily oxidizable into Fe^{3+} upon NO_2 adsorption, and this result has to be related to the intensity of the band corresponding to Fe^{3+}-OH (3680 cm^{-1} on Fig. 6A), which tends to be much less intense than in the case of Fe-H-BEA. Going on with the comparison of the maximum intensity reached by the ν(NO) band upon NO_2 adsorption over the two zeolitic samples (compare Fig. 3A inset with Fig. 6A inset), we notice that even if the Fe wt.% loading is twice for the Fe-H-ZSM-5, the nitrosyl maximum band intensity is similar. According to us, this either confirm that an important part of Fe^{2+} is not oxidizable and thus does not react with NO_2 providing the required NO to form nitrosyl species; or it may also point out that for the Fe-H-ZSM-5 sample, a main part of iron species remains in a stable oxidized form even after a vacuum activation at 673 K. Indeed, it seems rather difficult to avoid the formation of iron oxides nanoparticles inside the zeolite porous system upon increasing iron loading. A confirmation of this last hypothesis is suggested by the much higher intensity ratios I(1635)/I(1651) obtained for the Fe-H-ZSM-5, which indicates a higher amount of iron-containing nitrates: the iron oxide nanoparticles would provide supplementary sites for nitrates formation. Another explanation for the very low intensity of the Al-based nitro species (1651 cm^{-1}) lies in the higher amount of acidic OH groups (3610 cm^{-1}) detected after activation in the case of Fe-H-ZSM-5 (Fig. 1): NO_2 preferentially reacts with these OH groups to yield a higher amount of water and NO^+ species (2133 cm^{-1}) rather than with the alumina binder.

As a transition towards more realistic operando conditions, experiments were performed in order to investigate the influence of humidity on the adsorption process and thus on the nature of adsorbed species on the catalyst. Water was thus adsorbed on both Fe-H-BEA and Fe-H-ZSM-5 activated under vacuum and saturated with NO_2. We decided here to report only the data obtained for the later sample, since it is more hydrophilic and thus gives more representative results.

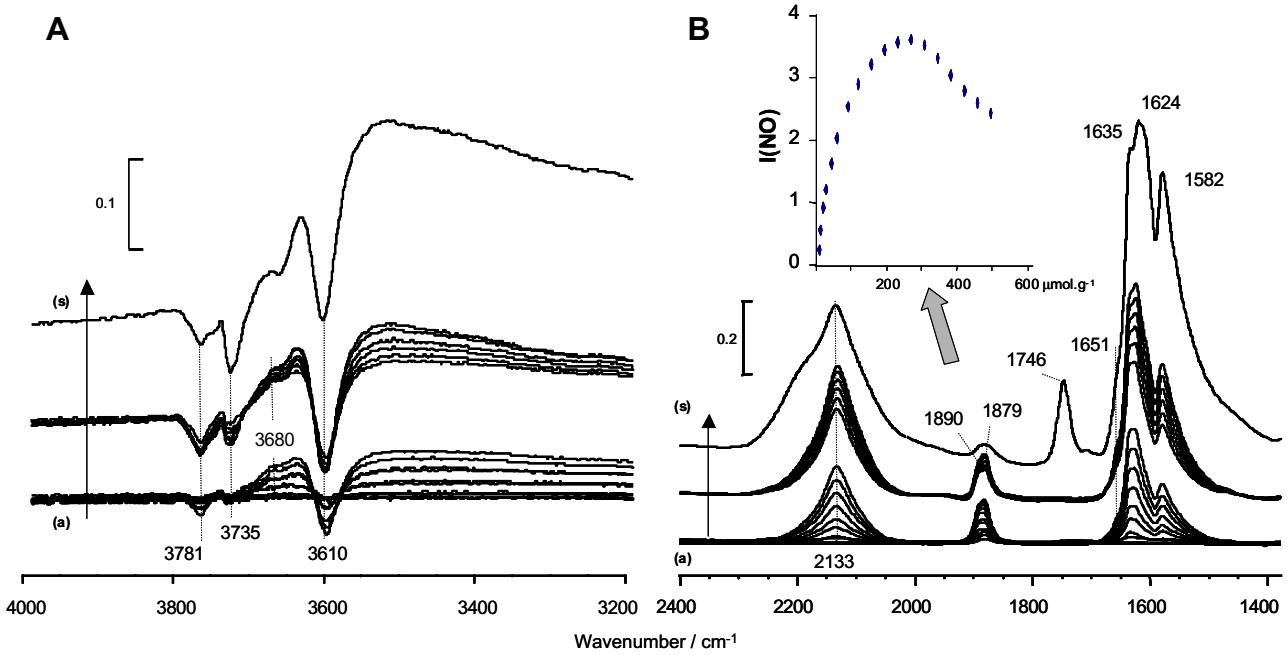

Fig. 6. FTIR spectra taken during the adsorption of NO_2 on Fe-H-ZSM-5 activated at 673 K under vacuum in the ν(OH) range (A) and in the (2400–1400 cm^{-1}) range (B) with the corresponding amount of introduced probe molecule: from (a) to (l) between 4 and 260 µmol g^{-1}; from (m) to (r) between 300 and 490 µmol g^{-1} and for (s) with an NO_2 equilibrium pressure of 266 Pa. The inset plot represents the evolution of the nitrosyl ν(NO) band intensity versus the amount of introduced NO_2.

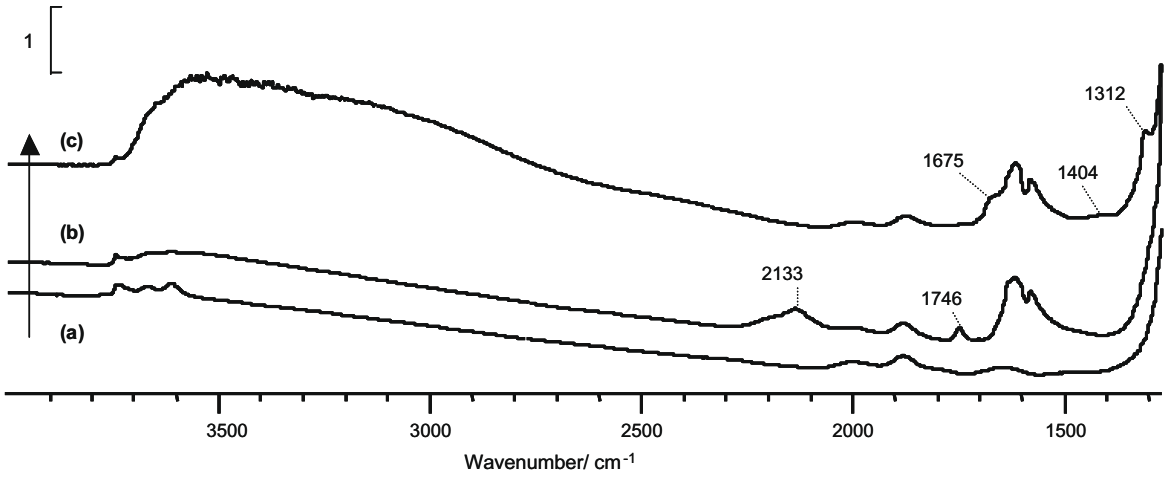

Fig. 7. Direct FTIR spectra of Fe-H-ZSM-5: (a) activated at 673 K under vacuum, (b) subsequently saturated with 266 Pa NO_2 equilibrium pressure and (c) with further 532 Pa H_2O equilibrium pressure.

It should be mentioned that the atmosphere in the cell still contained residual gaseous NO_2 in order to be as close as possible to the operando conditions. From Fig. 7, we can conclude that the addition of water has a strong effect on the bands corresponding to NO^+ (2133 cm^{-1}) and N_2O_4 (1746 cm^{-1}) (leading to their complete disappearance), while only small perturbations can be found for the nitro/nitrate species. Furthermore, three new bands are detected at 1675, 1404 and 1312 cm^{-1} that we confidently assign to adsorbed HNO_3 according to the literature [46]. Therefore, the nitrates present after NO_2 saturation are too stable to react with water, and the HNO_3 found at the surface should be formed according to the reaction:

$$N_2O_4 + H_2O \rightarrow HNO_3 + HONO \quad (8)$$

Indeed, traces of unstable HONO were detected in the gas phase which confirms this hypothesis. It should be taken into account that the pre-adsorbed N_2O_4 (see Fig. 3) is surely not the only source for HNO_3: as there is still residual NO_2 in the gas phase, its dissolution in condensed pseudo liquid water may also feed the same reaction path. Yeom et al. [48] previously described that NO_2 may disproportionate inside the zeolite micropores of BaNa-Y leading to the formation of NO^+ and NO_3^- which further react with water to yield HONO and HNO_3. These final products (nitrous and nitric acid) are common to the one we observed; however, our data do not allow to conclude that nitrates are involved in the acid formation. Nova et al. [49], on their way, report for V-based catalysts that the first step of the fast SCR consists in the formation of nitrous and nitric acid according to: $2NO_2 + H_2O \rightarrow HNO_3 + HONO$, which is also consistent with our finding.

4.2. Operando NO_2 adsorption

After the detailed characterization of the redox iron sites and their reactivity towards NO_2, the aim of this study was to test

our Fe-based zeolites as efficient alternatives to activated carbons for NO_2 trapping from atmospheric air. Correspondingly, operando experiments have been performed at 298 K. As these experiments have the intention to gain deeper insights into the performance of adsorbents under more realistic conditions, the samples were used without any activation and submitted to a flow made of NO_2, oxygen and moisture (or without moisture to investigate the influence of water on the catalyst performance) in proportion simulating NO_x polluted atmospheric air. The fact that NO species can be formed from NO_2 using both Fe-H-BEA and Fe-H-ZSM-5 under in situ conditions tends to be interesting due to the possibility to convert NO_2 into NO under flow. This would be of big toxicological interest, because NO is classified to be less harmful than NO_2.

It should be mentioned that such experiments using non-activated catalysts under flow and real conditions are quite rare, and only few examples exist in recent literature [37,50]. Thus comparison with corresponding literature data tends to be difficult. Dealing with the 20 wt.% γ-Al_2O_3 which was used as a binder in our samples, we can however refer to a reliable work from Szanyi et al. [44], who studied both the NO_2, H_2O and NO_2/water co-adsorption on this material. According to the nature of adsorbed species, our results obtained when making our blank experiment on the bare γ-Al_2O_3 were indeed fully consistent with the ones previously reported [44].

Fig. 8 shows a series of spectra recorded during the operando experiments performed at 298 K using Fe-H-BEA and Fe-H-ZSM-5. According to the band positions, HNO_3 (1680, 1410 and 1340 cm^{-1}) [46] and H_2O (1624 cm^{-1}) [36,46] are the main species observed for both samples during the adsorption process. This finding is in agreement with the previous results obtained from the in situ co-adsorption experiment (Fig. 7). Furthermore, it is remarkable that the nitrate species are the dominant stable species for the NO_x adsorption and water co-adsorption in situ experiments, whereas they only tend to play a minor role in operando (1562 cm^{-1} associated with alumina monodentate nitrate [44] remains negligible) when both components (NO_2 and H_2O) are sent together. More precisely, we must emphasize that in order to be as close as possible to the 'real life adsorbent conditions', we first stabilized the γ-Al_2O_3/zeolites porous system with the water containing flow before introducing NO_2 in the gas composition. The operando conditions are thus different from the ones applied in the in situ experiments: the NO_2 accessibility towards the adsorption/redox centers should then be limited by the diffusion through a water pseudo-liquid phase where different chemical reactions may take place. In Fig. 9, the gas phase results obtained from chemiluminescence during the experiment described in Fig. 8 are shown. Monitoring the signals for NO and NO_2 leads to the conclusion that the initial NO_2 amount (350 ppm) can be completely suppressed for a defined time, while NO is always produced and released with a proportion representing one third of the removed NO_2. In the presence of 60% relative humidity (1.7% H_2O), the NO_2 removal capacity (corrected from the blank with Al_2O_3) can be calculated after 7 h on stream to be 180 mg/g (120 mg/g as adsorbed species when taking into account the NO release) and 125 mg/g (90 mg/g as adsorbed species when taking into account the NO release) for Fe-H-BEA and Fe-H-ZSM-5, respectively.

Taking the previous qualitative results (HNO_3-adsorption and NO-formation) and semi-quantitative results ($NO_{2\ removed}$/$NO_{\ formed}$ = 3) into account, a reaction mechanism can be formulated from the operando experiment. HNO_3 initially is formed according to:

$$2NO_{2,(g)} + H_2O_{(ads.)} \rightarrow HNO_{3,(ads.)} + HONO_{(g)} \quad (9)$$

then HONO further reacts with NO_2 to form NO according to:

$$HONO + NO_2 \rightarrow HNO_3 + NO \quad (10)$$

Accordingly, for this mechanism also observed by Grossale et al. [51], 3 mol of converted NO_2 yield 1 mol of NO, and the amount of NO released thus corresponds to one third of the amount of NO_2 removed by the adsorbent (as experimentally observed). Another consequence of the proposed mechanism lies in the fact that H_2O should be crucial for the adsorption performance. Thus, different water amounts were introduced in the flow, and the corresponding chemiluminescence results are reported in Fig. 10 for the Fe-H-BEA sample.

It can be easily concluded that a positive water-effect exists, and the duration of the total suppression of NO_2 can be substantially increased by increasing the water amount in the flow (and thus increasing the amount of adsorbed water). More than a kinetic effect of water which would accelerate the process, the increment of NO_2 removal capacity seems rather to be due to the higher dissolution of NO_2 in a higher amount of water condensed inside the zeolite pores. The total amount of eliminated NO_2 therefore increases with humidity, and Table 2 summarizes the quantitative

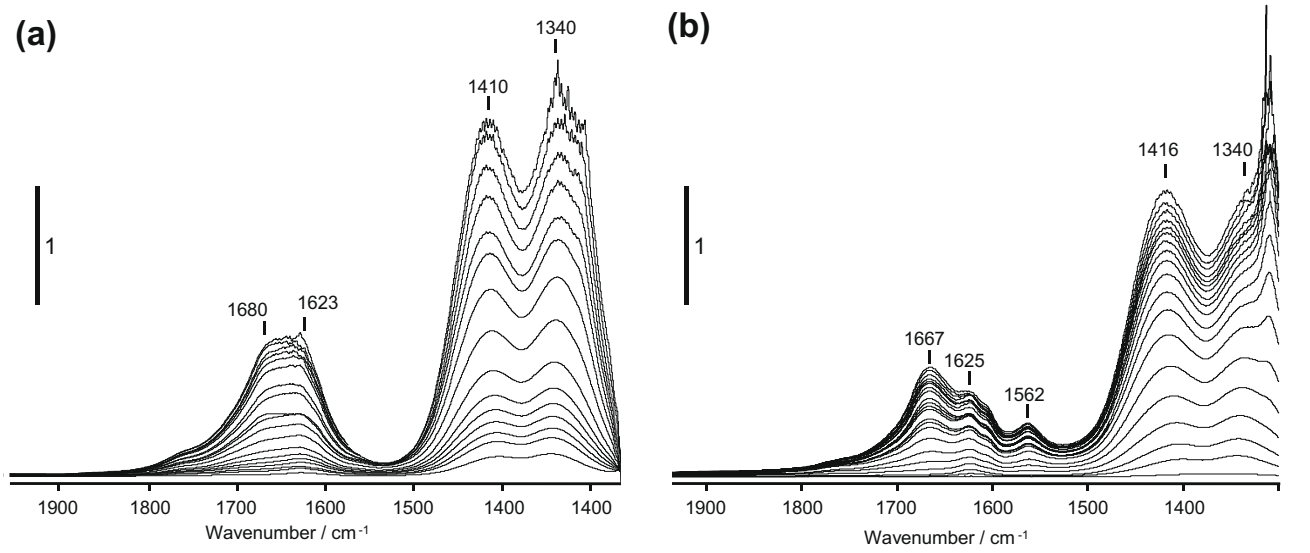

Fig. 8. Series of spectra during operando experiments using (a) Fe-H-BEA and (b) Fe-H-ZSM-5 in a flow of Ar, 20% O_2, 350 ppm NO_2 and 1.7% H_2O (total flow: 25 cm^3/min) at 298 K. The spectrum relative to the sample surfaces under H_2O at equilibrium was subtracted for clarity seek.

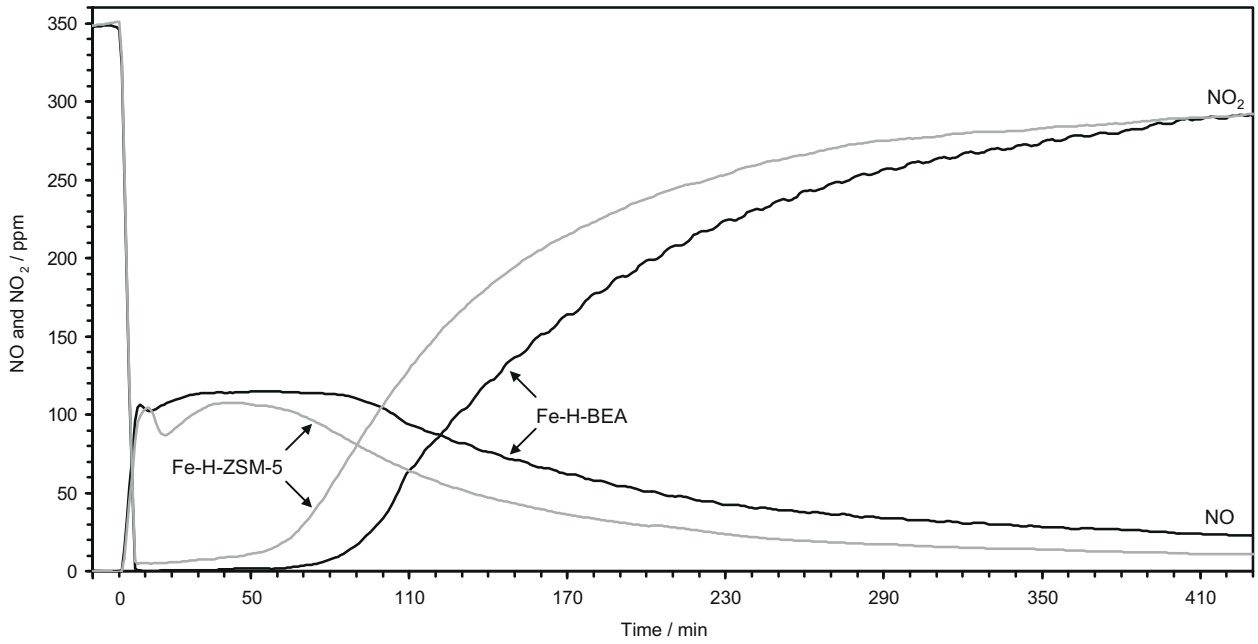

Fig. 9. Chemiluminescence results monitoring NO_2 and NO during operando experiments using, respectively 25.6 mg of Fe-H-BEA and 27.8 mg of Fe-H-ZSM-5, respectively, in a flow of Ar, 20% O_2, 350 ppm NO_2 and 1.7% H_2O (total flow: 25 cm^3/min) at 298 K.

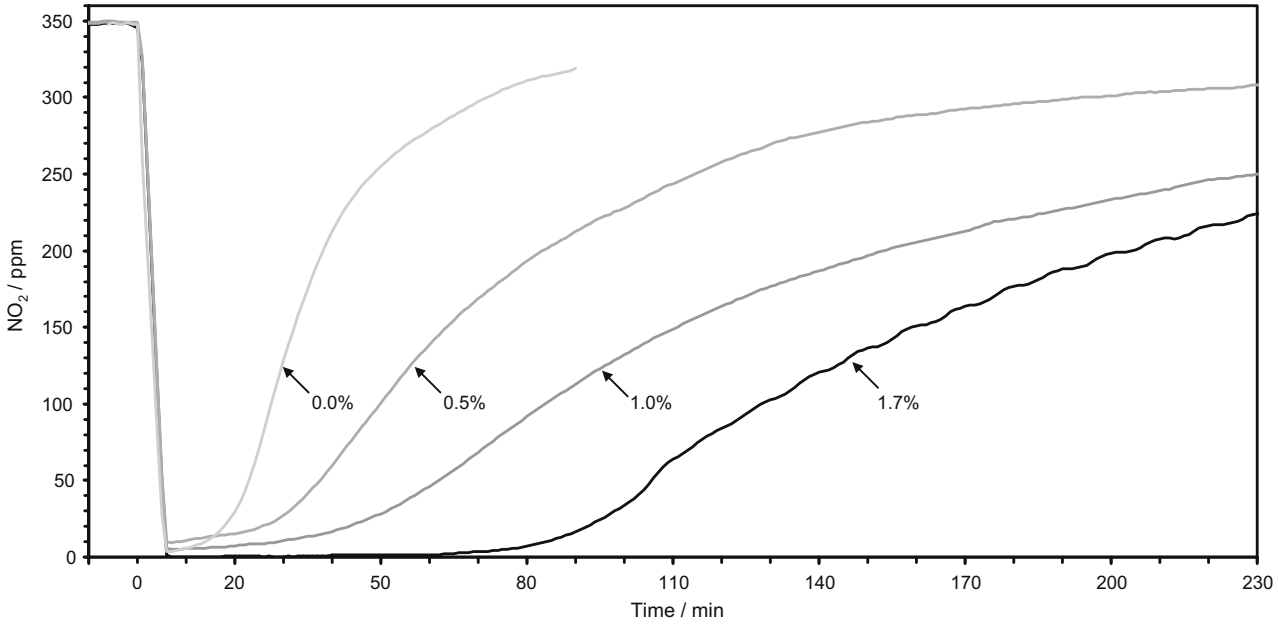

Fig. 10. Chemiluminescence results monitoring NO_2 during operando experiments using Fe-H-BEA at 298 K in a flow of Ar, 20% O_2, 350 ppm NO_2 and 0, 0.5, 1.0 and 1.7% H_2O (total flow: 25 cm^3/min). The sample weights were 33.0–22.0–20.4 and 25.6 mg for increasing water amounts.

Table 2
NO_2 removal efficiency at 298 K: a quantitative summary.

Sample	Fe-H-BEA				Fe-H-ZSM-5
Water content/vol.%	0	0.5	1	1.7	1.7
Removed NO_2/mg/g (corrected from Al_2O_3)	15	75	145	180	125
Adsorbed NO_2/mg/g (in the HNO_3 form and corrected from Al_2O_3)	10	50	100	120	90

results obtained for NO_2 removal with various samples/conditions. Such a stoichiometry indicating the disappearance of three NO_2 molecules from the gas phase to release one NO molecule was already described for Cu-ZSM-5 samples [50] in which trapped NO_x appear in the form of $Cu(NO_3)_2$. In that case, nitrates however appear to compete with water which was thus described to have a negative role on NO_2 removal efficiency.

Going back to the comparison between the total amount of removed NO_2 for adsorbents Fe-H-BEA and Fe-H-ZSM-5, one may also suggest that the main reason for a lower NO_2 removal efficiency (for Fe-H-ZSM-5) comes from a lower amount of pre-adsorbed water. Considering the hydrophilicity parameter only, we should not expect the observed ranking between Fe-H-BEA and Fe-H-ZSM-5, since the latter zeolite is aluminium richer than the

former and also possesses a higher iron loading. It thus appears here that the main parameter governing the water adsorption capacity (and thus further NO_2 removal efficiency) is the specific area which is double for the Fe-H-BEA sample.

A positive water-effect was thus detected, and this is remarkable since Despres et al. [50] also found a NO_2 to NO conversion during NO_2 adsorption using Cu-ZSM-5 as a catalyst, but in that case, a negative water-effect was on the contrary reported. Finally, we should mention that whatever the amount of water, the amount of NO released is always equal to 1/3 of the amount of NO_2 removed by the adsorbent. It may be surprising that this stoichiometry is preserved for a water-free feed. However, in order to be as close as possible from real conditions, our samples were never thermally activated, so that even for 'water-free gas feed', our samples always presented adsorbed water (probably condensed inside the microporous system) whose amount naturally increased when water was added in the gas flow. The NO_2 storage mechanism in the absence of H_2O in the gas flow is thus the same.

5. Conclusions

During the adsorption of NO_2 on Fe-H-BEA under in situ FTIR conditions, the well-known disproportion reaction leading to NO^+ and nitrate species was observed. Additionally, a redox reaction involving Fe^{3+}-OH and/or α-oxygen species leading to the formation of NO species was identified. This redox reaction is not only scientifically important, but may strongly influence the performance of the catalyst as the transformation of NO_2 into NO would be a substantial improvement from a toxicological point of view and would thus favour the use of zeolitic materials for indoor air treatment. In order to clarify this point and aiming to obtain complementary parameters such as adsorption capacities, further operando FTIR studies were performed.

According to the obtained operando FTIR results, NO is indeed formed for both Fe-H-BEA and Fe-H-ZSM-5, and the chemiluminescence data suggest that: (a) NO_2 can be completely suppressed for a defined time and (b) during all the period for which NO_2 is removed (even partially), 1 mol NO is released per 3 mol NO_2. Adsorbed HNO_3 was found to be the major species responsible for the storage of NO_2 and we obtained the following best removal efficiencies: 180 mg/g of catalyst (120 mg/g as adsorbed species when taking into account the NO release) and 125 mg/g of catalyst (90 mg/g as adsorbed species when taking into account the NO release) for Fe-H-BEA and Fe-H-ZSM-5, respectively. The proposed mechanism leading to adsorbed HNO_3 and respecting the observed stoichiometry relative to the formation of NO includes the consumption of water. Consequently, it was confirmed that the presence of water in the flow is crucial for a good performance: a positive water-effect was evidenced.

Combining these results, we conclude that the investigated zeolites (especially Fe-H-BEA) are promising candidates for further investigations in order to use such materials as filters in automotive air-conditioning systems. Translating the applied operando FTIR flow parameters into long-term stability makes clear that a regeneration process is not needed for these materials as a simple replacement of the filter during regular routine check-ups would be highly sufficient.

Acknowledgments

This work has been supported by the French Secretary for Industry (DGE department) and Region Lower Normandy within the project MADAIR (Nouveaux Médias Adsorbants pour la Purification de l'Air Habitacle).

References

[1] M. Petersson, J.K. Karlsson, Ambient Air Pollution Trap, Ford Global Technologies, LLC, Swed., US Application Patent: US, 2004, 13pp.
[2] M. Suzuki, Kagaku to Kogyo (Osaka, Japan) 80 (2006) 474.
[3] K. Partti-Pellinen, O. Marttila, A. Ahonen, O. Suominen, T. Haahtela, Indoor Air – International Journal of Indoor Air Quality and Climate 10 (2000) 126.
[4] X.X. Wang, X.L. Ma, S.Q. Zhao, B. Wang, C.S. Song, Energy & Environmental Science 2 (2009) 878.
[5] M. Maki, M. Suzuki, I. Kobayashi, Pellet for Nitrogen Oxide Removal, Matsushita Electric Industrial Co., Ltd., Japan, JP Application Patent: JP, 1976, 3pp.
[6] T. Yoshida, H. Ohta, K. Sugimoto, K. Kuwabara, T. Fukuta, Nenryo Kyokaishi 69 (1990) 1130.
[7] L. Pommer, J. Fick, B. Andersson, C. Nilsson, Atmospheric Environment 36 (2002) 1443.
[8] M.C. Wu, N.A. Kelly, Applied Catalysis B – Environmental 18 (1998) 79.
[9] T. Ibusuki, K. Takeuchi, Journal of Molecular Catalysis 88 (2004) 93.
[10] T. Ibusuki, Jidosha Gijutsu 50 (1996) 34.
[11] H. Takeuchi, N. Negishi, Kemikaru Enjiniyaringu 44 (1999) 964.
[12] K. Takeuchi, Kikan Kagaku Sosetsu 41 (1999) 205.
[13] M. Fukumoto, Yosha Gijutsu 20 (2000) 14.
[14] Y. Miyoshi, J. Hoshi, Tokyo-to Kankyo Kagaku Kenkyusho Nenpo (2000) 128.
[15] K. Takeuchi, H. Kobara, T. Sano, Ryusan to Kogyo 53 (2000) 37.
[16] T. Maggos, J.G. Bartzis, P. Leva, D. Kotzias, Applied Physics A – Materials Science & Processing 89 (2007) 81.
[17] L.G. Krishtopa, L.N. Krasnoperov, Journal of Advanced Oxidation Technologies 6 (2003) 30.
[18] S. Pasquiers, European Physical Journal: Applied Physics 28 (2004) 319.
[19] Y. Horii, T. Yamashita, A. Inoue, Nitrogen Dioxide Removal from Air Independently of Relative Humidity, Kobe Steel, Ltd., Japan, JP Application Patent: JP, 2000, 7pp.
[20] M.D. Lindsay, W.S. Lovell, Advances in Filtration and Separation Technology 15 (2002) 393.
[21] K. Ito, G.D. Thurston, A. Nadas, M. Lippmann, Measurement of Toxic and Related Air Pollutants, in: Proceedings of a Specialty Conference, Cary, NC, United States, vol. 1, September 1–3, 1998, p. 53.
[22] Q. Sun, Z.-X. Gao, H.-Y. Chen, W.M.H. Sachtler, Journal of Catalysis 201 (2001) 88.
[23] M. Devadas, O. Kröcher, M. Elsener, A. Wokaun, N. Söger, M. Pfeifer, Y. Demel, L. Mussmann, Applied Catalysis B: Environmental 67 (2006) 187.
[24] S. Brandenberger, O. Kröcher, A. Tissler, R. Althoff, Catalysis Reviews: Science and Engineering 50 (2008) 492.
[25] A. Grossale, I. Nova, E. Tronconi, D. Chatterjee, M. Weibel, Journal of Catalysis 256 (2008) 312.
[26] V. Blasin-Aube, O. Marie, J. Saussey, A. Plesniar, M. Daturi, N. Nguyen, C. Hamon, M. Mihaylov, E. Ivanova, K. Hadjiivanov, Journal of Physical Chemistry C 113 (2009) 8387.
[27] K. Hadjiivanov, Catalysis Review – Science Engineering 42 (2000) 71.
[28] I. Malpartida, E. Ivanova, M. Mihaylov, K. Hadjiivanov, V.B. Aubé, O. Marie, M. Daturi, Catalysis Today 149 (2010) 295.
[29] T. Wainman, C.J. Weschler, P.J. Lioy, J.F. Zhang, Environmental Science & Technology 35 (2001) 2200.
[30] C. Jia, P. Massiani, D. Barthomeuf, Journal of Chemical Society, Faraday Transactions 89 (1993) 3659.
[31] I. Kiricsi, C. Flego, G. Pazzuconi, W.O. Parker Jr., R. Millini, C. Perego, G. Bellussi, Journal of Physical Chemistry 98 (1994) 4627.
[32] A. Vimont, F. Thibault-Starzyk, J.C. Lavalley, Journal of Physical Chemistry B 104 (2000) 286.
[33] C. Yang, Q. Xu, Zeolites 19 (1997) 404.
[34] H. Knözinger, P. Ratnasamy, Catalysis Review – Science Engineering 17 (1978) 31.
[35] R. Kefirov, E. Ivanova, K. Hadjiivanov, S. Dzwigaj, M. Che, Catalysis Letters 125 (2008) 209.
[36] K. Hadjiivanov, J. Saussey, J.L. Freysz, J.C. Lavalley, Catalysis Letters 52 (1998) 103.
[37] R. Brosius, P. Bazin, F. Thibault-Starzyk, J.A. Martens, Journal of Catalysis 234 (2005) 191.
[38] M.S. Kumar, M. Schwidder, W. Grünert, U. Bentrup, A. Brückner, Journal of Catalysis 239 (2006) 173.
[39] G. Mul, J. Pérez-Ramírez, F. Kapteijn, J.A. Moulijn, Catalysis Letters 80 (2002) 129.
[40] C. Henriques, O. Marie, F. Thibault-Starzyk, J.C. Lavalley, Microporous and Mesoporous Materials 50 (2001) 167.
[41] O. Marie, N. Malicki, C. Pommier, P. Massiani, A. Vos, R. Schoonheydt, P. Geerlings, C. Henriques, F. Thibault-Starzyk, Chemical Communications (2005) 1049.
[42] F. Thibault-Starzyk, O. Marie, N. Malicki, A. Vos, R. Schoonheydt, P. Geerlings, C. Henriques, C. Pommier, P. Massiani, Studies in Surface Science and Catalysis 158 (2005) 663.
[43] G.M. Underwood, T.M. Miller, V.H. Grassian, Journal of Physical Chemistry A 103 (1999) 6184.
[44] J. Szanyi, J.H. Kwak, R.J. Chimentao, C.H.F. Peden, Journal of Physical Chemistry C 111 (2007) 2661.
[45] E.J.M. Hensen, Q. Zhu, R.A. van Santen, Journal of Catalysis 220 (2003) 260.

[46] A.L. Goodman, G.M. Underwood, V.H. Grassian, Journal of Physical Chemistry A 103 (1999) 7217.
[47] G. Mul, M.W. Zandbergen, F. Kapteijn, J.A. Moulijn, J. Pérez-Ramírez, Catalysis Letters 93 (2004) 113.
[48] Y.H. Yeom, J. Henao, M.J. Li, W.M.H. Sachtler, E. Weitz, Journal of Catalysis 231 (2005) 181.
[49] I. Nova, C. Ciardelli, E. Tronconi, D. Chatterjee, B. Bandl-Konrad, Catalysis Today 114 (2006) 3.
[50] J. Despres, M. Koebel, O. Kröcher, M. Elsener, A. Wokaun, Microporous and Mesoporous Materials 58 (2003) 175.
[51] A. Grossale, I. Nova, E. Tronconi, Catalysis Letters 130 (2009) 525.